Available online at www.sciencedirect.com
SCIENCE DIRECT®
Surface Science 536 (2003) 1–14
SURFACE SCIENCE
www.elsevier.com/locate/susc

Diffusion of particles adsorbed on a triangular lattice: pairwise and three-particle interactions

A.A. Tarasenko [a,b], F. Nieto [c,*], L. Jastrabík [b], C. Uebing [d]

[a] Institute of Physics, National Academy of Sciences of Ukraine, Prospect Nauki 46, UA-03039, Kyiv 39, Ukraine
[b] Institute of Physics, Academy of Sciences of the Czech Republic, Na Slovance 2, 182 21 Prague 8, Czech Republic
[c] Departamento de Física, Universidad Nacional de San Luis, CONICET, Chacabuco 917, 5700 San Luis, Argentina
[d] Department of Physics and Astronomy, Rutgers University, 136 Frelinghuysen Rd., Piscataway, NJ 08854-8019, USA

Received 12 April 2002; accepted for publication 10 April 2003

Abstract

In the present paper, the influence of both pairwise and three-particle interactions on the mobility of adsorbed particles diffusing on a lattice with triangular symmetry has been studied. Two different techniques has been used for describing the surface diffusion phenomenon.

On one hand, explicit expressions for the chemical and jump diffusion coefficients have been calculated by using real-space renormalization group (RSRG) approach. A number of the RSRG transformations with blocks of different sizes and symmetries have been investigated. In particular, it has been shown that the precision of the method depends strongly not only on the number of sites in the RSRG blocks but also on their composition and structure.

On the other hand, numerical simulations by using the Monte Carlo scheme has been used to simulate the process of particle migration. Using both methods, adsorption isotherms for different temperatures and the coverage dependencies for the thermodynamic factor and the chemical diffusion coefficient have been calculated. The behavior of the above mentioned quantities has been compared when the adparticles interact via only either pairwise or three-particle interactions.

Despite the fact that both methods constitute very different approaches, the correspondence of numerical data with analytical results is surprisingly good. Therefore, it can be concluded that the RSRG method can be successfully applied for lattice gas systems to characterize the thermodynamic and kinetic properties of strongly interacting adsorbates.
© 2003 Elsevier Science B.V. All rights reserved.

Keywords: Monte Carlo simulations; Surface diffusion; Ising models; Adsorption isotherms; Adsorption kinetics; Surface thermodynamics (including phase transitions)

1. Introduction

The migration of adsorbates on solid surfaces plays an essential role in many physical and chemical processes such as adsorption, desorption, melting, roughening, crystal and film growth, catalysis and corrosion, just to name a few [1–4].

* Corresponding author. Tel.: +54-2652-436151; fax: +54-2652-425109/430224.
E-mail address: fnieto@unsl.edu.ar (F. Nieto).

0039-6028/03/$ - see front matter © 2003 Elsevier Science B.V. All rights reserved.
doi:10.1016/S0039-6028(03)00599-5

Understanding surface diffusion is one of the keys for controlling these processes.

In recent years, the effects of lateral interactions between adsorbed particles on the collective surface diffusion coefficients have been intensively investigated using many different theoretical methods applicable to critical phenomena. In fact, mean-field [5–7], Bethe–Peierls [8], real-space renormalization group (RSRG) [9–11], Mori projection operator [12–14] and Monte Carlo (MC) [6,7,15–20] methods have been used to describe surface diffusion. It has been found that adparticle interactions can strongly influence surface diffusion, especially at low temperatures and in the close vicinity of surface phase transitions.

In general, the determination of the chemical surface diffusion coefficient requires the solution of a kinetic equation for a system of many particles. However, if one considers the slowly varying in space and time small disturbances of the adparticle surface coverage, the problem can be reduced to the calculation of purely thermodynamic quantities [3,21–23]. For this case, the problem of determining the adparticle diffusion coefficient is equivalent to the calculation of the system free energy.

The main aim of the present work is the investigation of the possibilities of the RSRG approach on lattices of triangular symmetry. For this purpose, a number of RSRG transformations with blocks of different sizes and symmetries have been generated. We have determined critical properties of 32 RSRG transformations for pure pair repulsive and attractive interactions and pure three-particle repulsive and attractive interactions. It was shown that the RSRG transformations for the triangular symmetry have some specific properties quite different from the main features of the RSRG transformations developed for square and honeycomb symmetries. Using the best RSRG transformations we have calculated different thermodynamical quantities: adsorption isotherms, the nearest neighbors pair correlation function and coverage dependences of the thermodynamic factor, tracer and chemical diffusion coefficients in a wide temperature range. All dependences, obtained by the RSRG method, have been checked by MC simulations showing very good coincidence even at very low temperatures.

The outline of this paper is as follows: the model, Hamiltonian and basic definitions are presented in Section 2. The main features of the RSRG approach are considered in Section 3. RSRG and MC results are discussed in Section 4. Finally, we give our conclusions in Section 5.

2. Basic definitions

In the following, we shall consider an ideal solid surface of triangular symmetry. The potential relief minima of the surface form a two-dimensional triangular lattice with lattice constant a, as shown in Fig. 1. Foreign particles, adsorbed on the surface, are assumed to exclusively occupy these sites. If the depth of these potential minima, ε, is much larger than the thermal energy, $k_{\mathrm{B}}T$, the adparticles will stay within the potential minima and from time to time perform jumps to the nearest neighbor empty sites (in the following we shall measure all energies in units of $k_{\mathrm{B}}T$). The duration of such a jump is much shorter than the mean time of an adparticle sojourn in a site. In this case, we can define a set of occupation numbers $\{n_i\}$ according to

$$n_i = \begin{cases} 1, & \text{if site } i \text{ is occupied,} \\ 0, & \text{if site } i \text{ is empty,} \end{cases} \tag{1}$$

describing completely all possible states of the adparticle system.

We suppose that adparticles interact with its nearest neighbors (nns) only. Then, the Hamiltonian of the system, H_a, and the total number of particles, N_a, can be written as follows

$$H_a = -\varepsilon N_a + \varphi \sum_{ij} n_i n_j + \psi \sum_{ijk} n_i n_j n_k,$$
$$N_a = \sum_i n_i. \tag{2}$$

Here φ and ψ are the pair and three nn particle interaction energies, respectively; symbols ij and ijk denote summation over all bonds and the elementary triangles of the lattice just once. The free energy (per site), f, is defined as follows

$$f = N^{-1} \ln \left\{ \sum_{\{n_i\}} \exp[\mu N_a - H_a] \right\}. \tag{3}$$

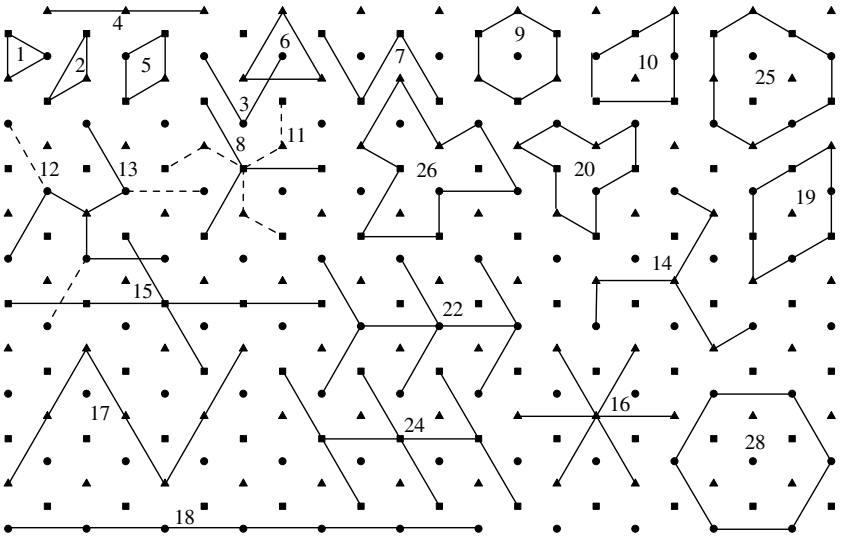

Fig. 1. Triangular lattice divided into three sublattices. Cell and sublattice RSRG blocks investigated in the paper are shown.

The summation in Eq. (3) is carried out over all 2^N configurations of the system of adparticles.

It should be noted that the three-particle interaction has a clear physical interpretation. At first glance, it looks quite different as compared with the ordinary pair–particle interaction but the physical reason which produces the both type of interactions is the same. The interaction between an adparticle and the surface changes not only the energy of the particle but also its physical properties. A big energy ε means that the interaction of an adparticle with the surface is strong which in turn also means a noticeable redistribution of the electronic density around the adparticle. Another adparticle produces its own disturbance of the electronic density. The interference between these disturbances, changing the adsorption energies, is equivalent to the lateral interaction between the particles. The total energy of the system of adparticles depends not only on the total number of adparticles but also on their configuration. Thus the energy can be expanded in series of different configurations: one-particle, different pairs of adparticles, different three-particles configurations and so on. We consider here the contributions resulted from the nn pair and three-particles configurations.

The occupation numbers are changed with time due to the jumps of adparticles. Different diffusion coefficients have been defined in order to describe the adparticle migration. Conceptually the simplest diffusion coefficient is a single particle or tracer diffusion coefficient, D_t, which is related to the asymptotic behavior of the mean square displacements of tagged particles. In this case, adparticles rather than lattice sites must be labeled. The tracer diffusion coefficient is defined as follows

$$D_t = \lim_{t\to\infty} \frac{1}{2dt} \left\langle [\vec{r}_i(t) - \vec{r}_i(0)]^2 \right\rangle, \tag{4}$$

where d is the system dimension ($d = 2$ in the case of surface diffusion) and $\vec{r}_i(t)$ is the displacement of the ith adparticle at time t.

The chemical diffusion coefficient is determined by the Fick's first law, which constitutes a linear relationship between the flux of adparticles, $\vec{J}(\vec{r},t)$, and the gradient of the adparticle surface coverage, $\theta(\vec{r},t)$

$$\vec{J}(\vec{r},t) = -D_c \vec{\nabla}\theta(\vec{r},t). \tag{5}$$

A suitable expression for the chemical diffusion coefficient, D_c, can be obtained in the local equilibrium approximation. We suppose that adparticles migrate over the surface, jumping from time to

time to the nn empty sites only. There is no correlation between adparticle jumps. Interested readers are referred to Refs. [10,23] for a detailed description of this approach. The expression for D_c can be written as follows

$$D_c = D^0 \exp(\mu) P_{00}/\chi_T. \quad (6)$$

Here $D^0 = 3va^2 \exp(-\varepsilon)/2$ is the diffusion coefficient of noninteracting adparticles on a triangular lattice; χ_T is the isothermal susceptibility and P_{00} is the probability of finding two nn holes (empty sites).

It is possible to calculate all quantities entering Eq. (6) via the corresponding first and second derivatives of the free energy, f, over the chemical potential, μ, and the pair interaction parameter, φ:

$$\theta = \frac{\partial f}{\partial \mu}, \quad \langle n_0 n_1 \rangle = -\frac{1}{3}\frac{\partial f}{\partial \varphi},$$
$$\chi_T = \frac{\partial^2 f}{\partial \mu^2}, \quad P_{00} = 1 - 2\theta + \langle n_0 n_1 \rangle. \quad (7)$$

Here the angular brackets $\langle \cdots \rangle$ denote averaging over all possible states of the system.

Thus, the calculation of the chemical diffusion coefficient is reduced to the evaluation of the free energy f of the lattice gas system. However, it is important to recall that the expression for the chemical diffusion coefficient was derived in the hydrodynamic limit (i.e. for adparticle coverage varying slowly in space and time). The characteristic size of the coverage disturbances should be much greater than the adparticle jump, a, and the characteristic time should exceed considerably the mean time of an adparticle sojourn in a site.

3. Real-space renormalization group transformations

In order to determine the free energy of the system, f, it is necessary to use some approximate methods. Even for the simplest models, the problem remains too complex to be solved exactly.

RSRG approach has been applied for the calculations of the free energy and its corresponding derivatives. The detailed description of the RSRG approach can be found elsewhere [24–29].

In this work, we have investigated 32 RSRG transformations with block size varying from 3 to 13 lattice sites, shown in Figs. 1 and 2. There are two possible ways of dividing lattices into blocks. The whole lattice can be divided into polygons (cells or blocks) of equal form and size. In this case, every block contains sites from different sublattices (recall that a triangular lattice may be regarded as composed of three equivalent sublat-

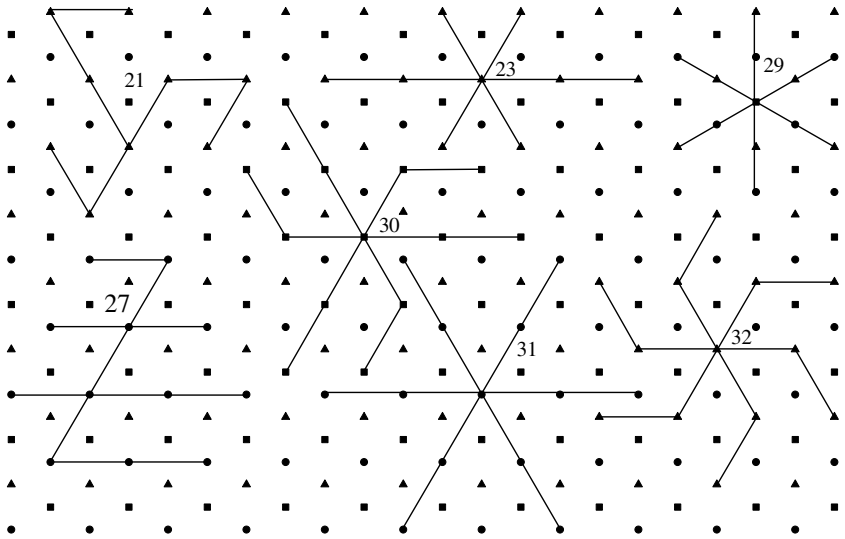

Fig. 2. The sublattice RSRG blocks investigated in the paper.

tices). Such type of blocks is used in the so-called *cell* RSRG transformations, which are denoted as $L \times 3$. These blocks are shown as polygons in Fig. 1. All sites in the polygon perimeter enter the block.

Another alternative method was suggested by Schick et al. [30]. In this approach the sublattices are divided into blocks of equal form and size. Any block contains sites from a single sublattice only. The cluster of three interpenetrating blocks from three different sublattices has also $3L$ sites but the value of any block spin is determined by the spins of a definite sublattice. In this case, the RSRG transformations are denoted as $L \times 3S$ (*sublattice* RSRG transformations). These blocks are drawn as graphs or snowflakes in Figs. 1 and 2, to show clearly which sites enter the block.

It is also possible to build blocks which are neither separate cells, not pure sublattice blocks. These blocks contain sites from different sublattices and partially interpenetrate each other. They have compositions where most of the sites belong to one sublattice with some admixture of sites from other sublattice(s).

We have used finite lattices consisting of three block sites with periodic boundary conditions. The lattices are built by a periodic continuation of clusters having $3L$ sites (or 3 block sites). It should be also noted that for RSRG calculations it is suitable to use the spin representation instead of occupation numbers. In spin language the pair attraction between adparticles corresponds to the ferromagnetic Ising model (F) while the repulsive interaction is equivalent to the antiferromagnetic behavior (AF). The three-particle interaction corresponds to the three-spin Baxter–Wu (BW) model [31].

In the following, some general properties of the RSRG transformations will be discussed. The cell $L \times 3$ RSRG transformations have better critical parameters in the F region as compared with the sublattice RSRG transformations. All pure cell RSRG transformations have a fixed point in the F region only. The critical value of the interaction parameter p_c approaches its exact value p^* if the number of sites in the block is increased. The accuracy of the RSRG transformations in the F domain decreases as one decreases the admixture of spins from different sublattices in the block, making its composition more uniform. Simultanously, the critical properties of the transformation in the AF and BW regions are improved. The accuracy of the RSRG transformations depends considerably not only on the block size L, but also on its composition, i.e. how many sites from different sublattices enter into the block. Really, the block size, its symmetry and composition are not independent variables. It is hard to estimate definitely the influence of the block symmetry and its composition on the critical properties. But in some cases it is possible to build blocks with the same size and different symmetries and compositions. Actually, there is a strong dependence of the critical parameters on the block composition. The symmetry of the blocks does not play important role for the sublattice $L \times 3S$ RSRG transformations.

One can consider, for example, the sequence of the RSRG transformation with $L = 7$ (blocks 9–18 in Figs. 1 and 2). All these transformations use clusters with the same number of sites from all three sublattices (7×3), but the sites are distributed between blocks in different proportions. The RSRG transformation with blocks, containing sites from all three sublattices does not show any AF and BW ordering, but has the best critical parameters in the F region among the 7×3 transformations. The block 9, has the perfect hexagon symmetry and the best critical values. The asymmetrical pentagon (#10) has slightly worse values. Blocks 11–14 include sites from two sublattices only. They have decreased the accuracy of the F critical parameters. Blocks 11–13 have almost uniform composition with only one site from another sublattice. The accuracy is low but they describe the AF ordering. Pure sublattice blocks (15–18 for example), have the lowest accuracy in the F region, but the best AF and BW critical parameters. Despite the fact that these blocks are rather different, all critical parameters are the same. A similar behavior is observed also for other sequence of blocks with $L = 13$ (#29–32). It seems that for the sublattice RSRG transformations the block symmetry has minor effect. Such behavior of cell and sublattice RSRG transformations differs considerably from the case of square lattice [11]. In

this case, the RSRG transformations works in both regions F and AF interaction with almost equal accuracy.

The cell $L \times 3$ RSRG transformations describe the F behavior with rather good accuracy. The sublattice RSRG transformations (for example, flakes 30–32 in Fig. 2) produce the best results for repulsive and three-particle interactions.

The critical parameters for all RSRG transformations are compiled in Tables 1 and 2. We have calculated critical values of the pair, p_c, and three-particle, t_c, interaction parameters, and corresponding critical exponents y_h, y_T and y_3. It should be noted that for all RSRG transformations the third critical exponent is irrelevant ($y_3 < 0$) in the F critical point and does not influence the critical dependencies of the thermodynamic quantities. We have also calculated the critical values of the entropy S_c and the internal energy U_c. These values are also known with great accuracy [32]. The critical values of the above mentioned parameters approach their exact values if the number of sites

Table 1
Compilation of the ferromagnetic critical values for the different clusters studied in the present work

#	Cluster	p_c	ϵ_F	y_h	y_T	y_3	S_c/k_B	$-U_c$	s_0	
	Exact	0.2747		1.875	1.0		0.330	0.549	0.323	
1	3×3	0.243	11.4	1.76	0.86	−1.2	0.439	0.378	0.299	1:1:1
2	3×3	0.229	16.4	1.70	0.82	−1.4	0.488	0.301	0.324	2:1:0
3	$3 \times 3S$	0.185	32.7	1.45	0.64	−1.1	0.612	0.124	0.324	3:0:0
4	$3 \times 3S$	0.185	32.7	1.45	0.64	−1.1	0.612	0.124	0.324	3:0:0
5	4×3	0.2732	0.52	1.85	0.90	−1.0	0.337	0.541	0.333	2:1:1
6	4×3	0.2737	0.36	1.86	0.89	−0.9	0.326	0.552	0.387	3:1:0
7	$4 \times 3S$	0.198	27.8	1.62	0.42	−0.8	0.596	0.194	0.374	4:0:0
8	$4 \times 3S$	0.203	26.3	1.62	0.4	−0.7	0.593	0.204	0.358	4:0:0
9	7×3	0.254	7.35	1.79	0.9	−0.9	0.411	0.428	0.322	3:3:1
10	7×3	0.251	8.7	1.77	0.9	−1.0	0.426	0.406	0.318	3:2:2
11	7×3	0.232	15.5	1.67	0.81	−1.4	0.499	0.302	0.325	4:3:0
12	7×3	0.220	20.0	1.59	0.72	−1.3	0.538	0.245	0.324	6:1:0
13	7×3	0.220	20.0	1.59	0.72	−1.3	0.538	0.245	0.324	6:1:0
14	7×3	0.231	15.7	1.66	0.80	−1.2	0.501	0.299	0.324	4:3:0
15	$7 \times 3S$	0.197	28.3	1.43	0.57	−1.2	0.595	0.162	0.324	7:0:0
16	$7 \times 3S$	0.197	28.3	1.43	0.57	−1.2	0.595	0.162	0.325	7:0:0
17	$7 \times 3S$	0.197	28.3	1.43	0.57	−1.2	0.595	0.162	0.325	7:0:0
18	$7 \times 3S$	0.197	28.3	1.43	0.57	−1.2	0.595	0.162	0.325	7:0:0
19	9×3	0.255	7.34	1.78	0.90	−0.9	0.415	0.425	0.320	3:3:3
20	9×3	0.253	8.06	1.77	0.89	−0.9	0.423	0.413	0.355	3:3:3
21	$9 \times 3S$	0.200	27.1	1.43	0.55	−1.2	0.589	0.174	0.326	9:0:0
22	$9 \times 3S$	0.200	27.1	1.43	0.55	−1.2	0.589	0.174	0.326	9:0:0
23	$9 \times 3S$	0.202	26.6	1.43	0.54	−1.2	0.585	0.180	0.326	9:0:0
24	$9 \times 3S$	0.200	27.1	1.43	0.55	−1.2	0.589	0.174	0.326	9:0:0
25	12×3	0.256	6.6	1.79	0.91	−0.9	0.410	0.433	0.319	4:4:4
26	12×3	0.250	9.1	1.75	0.87	−0.9	0.439	0.392	0.321	4:4:4
27	$12 \times 3S$	0.203	26.0	1.43	0.5	−1.1	0.586	0.185	0.325	12:0:0
28	13×3	0.257	6.27	1.79	0.91	−0.8	0.407	0.439	0.324	7:3:3
29	13×3	0.251	8.51	1.75	0.87	−0.9	0.434	0.400	0.324	6:6:1
30	$13 \times 3S$	0.205	25.3	1.42	0.51	−1.2	0.580	0.191	0.324	13:0:0
31	$13 \times 3S$	0.205	25.3	1.42	0.51	−1.2	0.580	0.191	0.324	13:0:0
32	$13 \times 3S$	0.205	25.3	1.42	0.51	−1.2	0.580	0.191	0.324	13:0:0

The first column shows the number of the block in Figs. 1 and 2 and the second is the corresponding RSRG transformations. p_c is the value of the spin pair interaction parameter p in the F critical point; y_h, y_T, y_3 are the corresponding critical exponents; ϵ_F is the relative error of the critical value of the pair interaction parameters in %; S_c and U_c are the values of entropy and internal energy in the critical point; s_0 is the entropy of the ground state. The last column is the composition of the blocks. The known exact values of the critical parameters are shown in the first line.

Table 2
Compilation of the critical values for the different clusters studied in the present work

#	Cluster	t_c	ϵ_{BW}	y_1	y_2	y_3	$\lvert p_{min}\rvert$	a_h	θ_c
	Exact	0.4407						1.20	0.276
3	$3\times 3S$	±0.741	68.2	2.00	0.55	−0.6	0.713	0.91	0.25
4	$3\times 3S$	±0.741	68.2	2.00	0.55	−0.6	0.713	0.91	0.25
12	7×3	±0.583	32.3	1.99	0.82	−0.2	0.861	1.64	0.315
13	7×3	±0.583	32.3	1.99	0.82	−0.2	0.861	1.64	0.315
15	$7\times 3S$	±0.558	26.7	1.99	0.85	−0.1	0.802	1.312	0.293
16	$7\times 3S$	±0.558	26.7	1.99	0.85	−0.1	0.802	1.312	0.293
17	$7\times 3S$	±0.558	26.7	1.99	0.85	−0.1	0.801	1.312	0.293
18	$7\times 3S$	±0.558	26.7	1.99	0.85	−0.1	0.801	1.312	0.293
22	$9\times 3S$	±0.533	20.9	1.99	0.90	0.07	0.854	1.76	0.319
23	$9\times 3S$	±0.529	20.0	1.99	0.92	0.01	0.818	1.46	0.305
24	$9\times 3S$	±0.533	20.9	1.99	0.90	0.06	0.851	1.76	0.319
27	$12\times 3S$	±0.501	13.7	1.98	1.00	0.11	0.786	1.37	0.299
30	$13\times 3S$	±0.498	13.0	1.42	0.51	−1.2	0.784	1.37	0.298
31	$13\times 3S$	±0.498	13.0	1.42	0.51	−1.2	0.784	1.37	0.298
32	$13\times 3S$	±0.498	13.0	1.42	0.51	−1.2	0.784	1.37	0.298

The first column shows the number of the block in Figs. 1 and 2. The second one is the corresponding RSRG transformations. t_c, ϵ_{BW}, y_1, y_2, y_3 are the critical value of the three-particle interaction parameter t, relative error in % and critical exponents of the BW phase transition; $|p_{min}|$ is the value of the pair interaction parameter corresponding to the maxima on the phase diagram in the plane $t = 0$; a_h and θ_c are the slope of the critical line at zero temperature and the corresponding surface coverage.

in the block L is increased. However, the accuracy of the RSRG transformation is not a monotone function of the block size L. As it was mentioned, for blocks with even L one must introduce an additional condition in order to determine the block spin for the spins configurations with zero sum. For blocks with even L, we have used a simple rule: the block spin for the zero sum configurations is determined by a value of some definite spin in the block. This condition gives an additional degree of freedom for improving the accuracy of the RSRG transformations with even L. We have tested all possibilities for blocks with $L = 4$ and only the best results are shown in Table 1. Depending on the chosen spin, the accuracy in determining the critical value of the pair interaction parameter is changing from 16% to 0.36% for triangles (block 6 in Fig. 1) and from 8% to 0.52% for rhombs (block 5 in Fig. 1). For triangle blocks the additional rule is the following: the block spin is equal to the negative value of the central site spin. The small total number of configurations makes the results very sensitive to the distribution of the zero sum configurations between domains.

All RSRG transformations (and RSRG calculations) have been carries out by using ordinary PC. It is a rather simple method with easy implementation, without any heavy requirements on memory and performance of computer used for the calculations. The accuracy of RSRG transformations with the smallest possible blocks ($L = 3$) is low. But transformations with bigger blocks produce results with accuracy satisfactory for many purposes.

4. Results and discussion

We have calculated some thermodynamic quantities necessary for determining the chemical diffusion coefficients using the best RSRG transformations. The data are obtained in the monolayer region of surface coverage and for a very wide temperature range. We have considered pure pair attraction and repulsion and pure three-particle attractive and repulsive interactions. Results of RSRG calculations have been compared with the corresponding data obtained by MC simulations (details of MC method are presented in Ref. [20]).

At first, we have calculated the adsorption isotherms (the first derivative of the free energy over the chemical potential, $\theta(\mu)$). Results obtained by

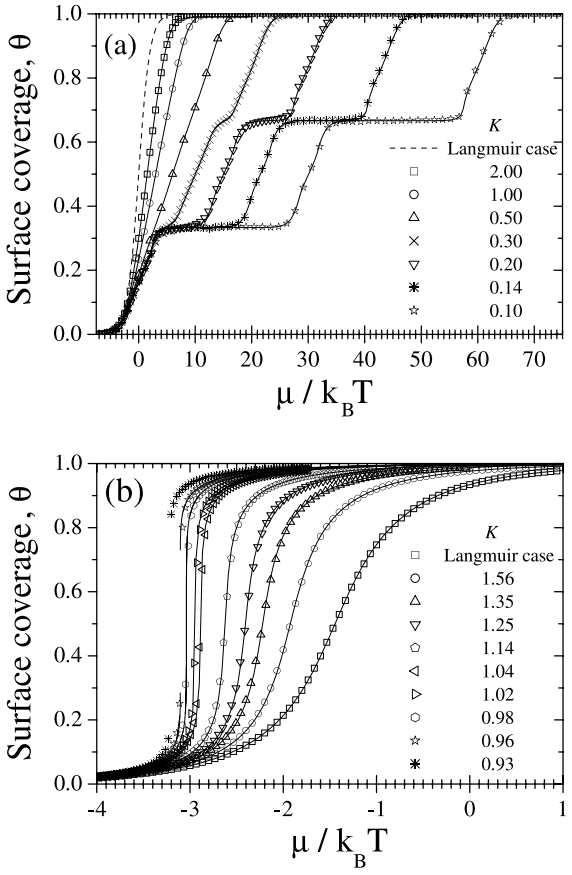

Fig. 3. Adsorption isotherms: surface coverage, θ, vs. μ/k_BT for different temperatures expressed in units of $K = k_BT/|\varphi|$ as indicated. Pair interaction: (a) repulsion, (b) attraction. Solid lines are obtained by the RSRG method, symbols denote MC data.

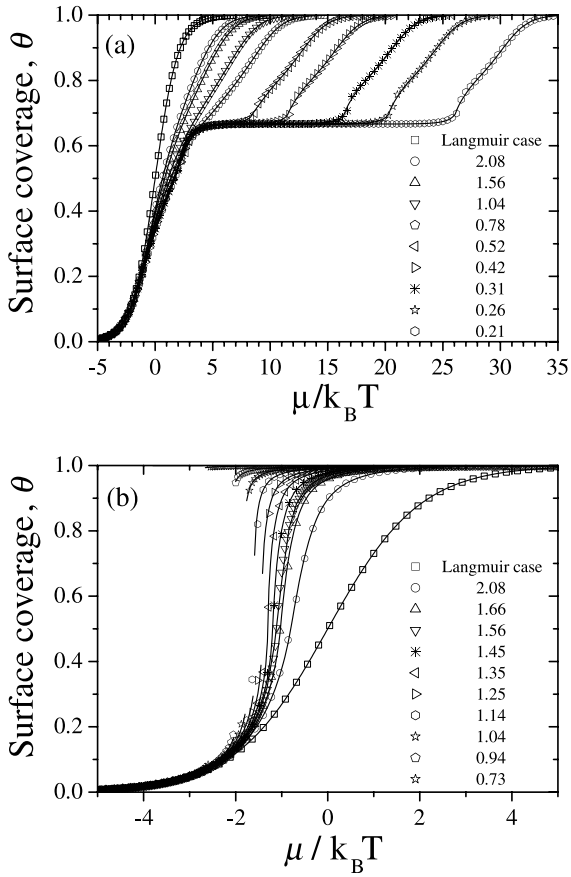

Fig. 4. Adsorption isotherms for different temperatures expressed in units of $K = k_BT/|\psi|$ as indicated. Pure three-particle interaction: (a) repulsion, (b) attraction. Solid lines and symbols denote the RSRG and MC data, respectively.

RSRG (solid lines) and MC methods (symbols) are shown in Figs. 3 and 4 for pairwise and three-particle interactions, respectively. At high temperatures isotherms are close to the Langmuir case (lattice gas without lateral interaction). For pairwise and three-particle repulsive interactions, the adsorption isoterms present clearly defined plateaus. In the former case the plateaus are located at $\theta = \frac{1}{3}$ and $\theta = \frac{2}{3}$, see Fig. 3a, while in the latter the isotherm present just one plateau at $\theta = \frac{2}{3}$ in the low temperature range shown in Fig. 4a. In all the cases considered these peculiar behavior corresponds to the AF ordered structures. Strong enough repulsion produces ordered phases when particles occupy preferentially sites of a single sublattice ($\theta = \frac{1}{3}$), or two sublattices ($\theta = \frac{2}{3}$). For pure pair repulsion between adparticles the regions of existence of these phases are placed symmetrically about $\theta = \frac{1}{2}$. The three-particle interaction destroys the symmetry inhibiting one AF ordered phase (centered at $\theta = \frac{1}{3}$ for $t = -\psi/8 < 0$) and expanding the region of existence for the other phase. Such behavior corresponds to the second order phase transitions.

Attractive interactions produce another kind of peculiarities. If temperature decreases, the adsorption isotherms became steeper at $\theta = \frac{1}{2}$ for the pair (Fig. 3b) and at $\theta = \frac{2}{3}$ for the three-particle attractive interactions (Fig. 4b). At the critical

temperature the isotherms have vertical tangents at the corresponding coverages. As temperature drops below critical, the dependencies became discontinuous. The behavior is typical for the first order phase transitions, when the mean surface coverage changes abruptly at some value of the chemical potential.

In all the cases considered here, the coincidence between RSRG and MC data is very good over the whole range of temperatures and surface coverages.

The quantity being the most sensitive to the phase transitions is the thermodynamic factor, T_f, which is related to the isothermal susceptibility χ_T (mean square surface coverage fluctuations) by the relationship:

$$T_f = \frac{\partial \mu}{\partial \ln \theta} = \frac{\theta}{\chi_T}. \quad (8)$$

The coverage dependencies of the thermodynamic factor are plotted in Figs. 5 and 6 for pairwise and three-particle interactions, respectively. For high temperatures (Langmuir case) the thermodynamic factor is equal to $1/(1-\theta)$. At low temperatures and for repulsive interactions, the density fluctuations are strongly suppressed at the stoichiometric coverages $\theta = \frac{1}{3}$ and $\theta = \frac{2}{3}$ in the case of pairwise interactions (Fig. 5a) and at $\theta = \frac{2}{3}$ for three-particle interactions (Fig. 6a). Any density disturbance (i.e. the displacement of an adparticle from its stable position in the filled sublattice to any site of the empty sublattice) substantially increases the free energy of the system and is thermodynamically unfavorable. As the coverage is not equal to (a) either one third or two thirds of a monolayer in the case of pairwise

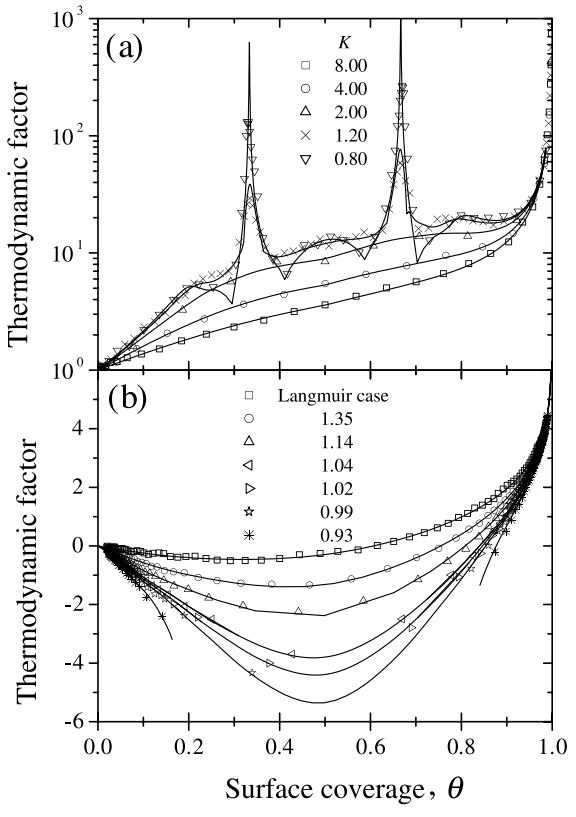

Fig. 5. The coverage dependencies of the thermodynamic factor for different temperatures. Notations are the same as in Fig. 3.

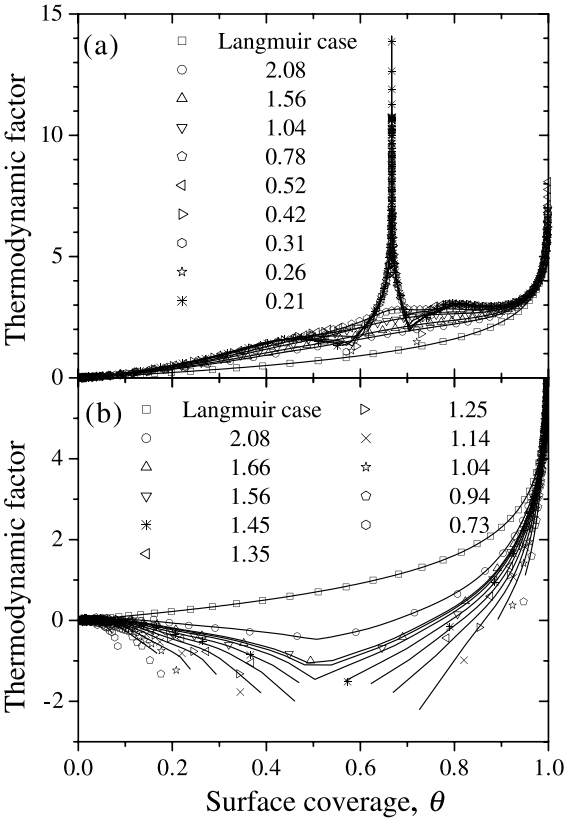

Fig. 6. The coverage dependencies of the thermodynamic factor for different temperatures. Notations are the same as in Fig. 4.

repulsive interactions and (b) two thirds for pure three-particle repulsive interactions; there are fluctuations of non-stoichiometric nature that do not require additional energy for their existence and cannot be removed from the system due to jumps of adparticles. Therefore, T_f increases when θ is approaching to such coverages. In fact, the coverage dependencies of T_f have high and narrow maxima at these coverages but remain analytical. In addition, the thermodynamic factor exhibits minima when the system cross the critical lines $T_c(\theta)$. The dependence of T_f in these points is nonanalytic. There are a good coincidence between RSRG and MC data in the whole coverage range for different temperatures excluding the vicinities of the critical points.

In the low temperature regime, attractive interactions cause the averall growing of the coverage fluctuations, keeping adparticles together and decreasing the relaxation of the coverage disturbances. The adparticle density fluctuations exhibit a sharp maximum at half coverage, growing to infinity as $T \to T_c$. In contrast, the thermodynamic factor exhibits a strong minimum, see Figs. 5b and 6b. Any surface coverage disturbance relaxes slower and slower as the lateral interactions between adparticles tends to its critical value. The system becomes unstable in the critical point and the fluctuations are strongly divergent. The critical behavior of the isothermal susceptibility is described by the following scaling dependence

$$\chi_T \sim (T - T_c)^{-\gamma} \quad \text{as } T - T_c \to +0, \quad \theta = 0.5. \quad (9)$$

One can determine easily the critical exponent γ by using the RSRG values for y_T and y_h listed in Table 1 and the relationship

$$\gamma = \frac{2(y_h - 1)}{y_T}. \quad (10)$$

The same critical exponent γ describes the critical slow down of the thermodynamic factor, T_f, and the chemical diffusion coefficient, D_c.

We shall proceed to the analysis of the coverage dependence of the normalized tracer diffusion coefficient which is plotted in Figs. 7 and 8 for the pair and three-particle interactions, respectively. In the both figures, the part (a) represents the case of attractive interactions while in part (b) the case

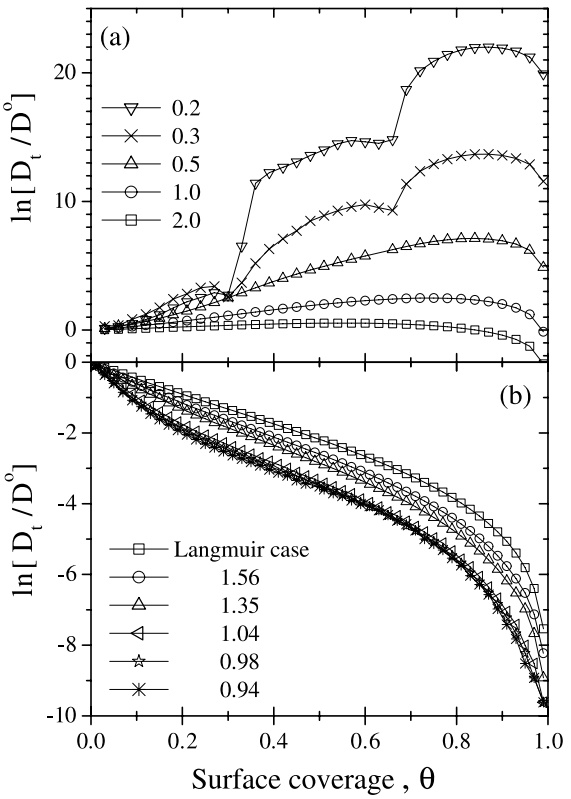

Fig. 7. The coverage dependencies of the tracer diffusion coefficient for different temperatures and pair interaction. Notations are the same as in Fig. 3. The data are obtained by the MC method.

of pure repulsive interactions is presented. The MC data for D_t/D^0 have been obtained for some representative temperatures. From a first qualitative inspection, it is obvious that repulsive interactions between adparticles cause a dramatic speed up of surface diffusion especially at low temperatures and high coverages. For the highest temperature shown in Figs. 7a and 8a, the tracer diffusion coefficient decreases monotonically with θ. Such behavior is typical for the Langmuir case. Deviations from the Langmuir behavior are strongly pronounced at low temperatures where repulsive interactions force the system to the second order phase transitions.

At low coverages (where the adatoms are far apart on average) the accelerating effect of the repulsive interactions is much less pronounced. At low temperatures the tracer diffusion coefficient,

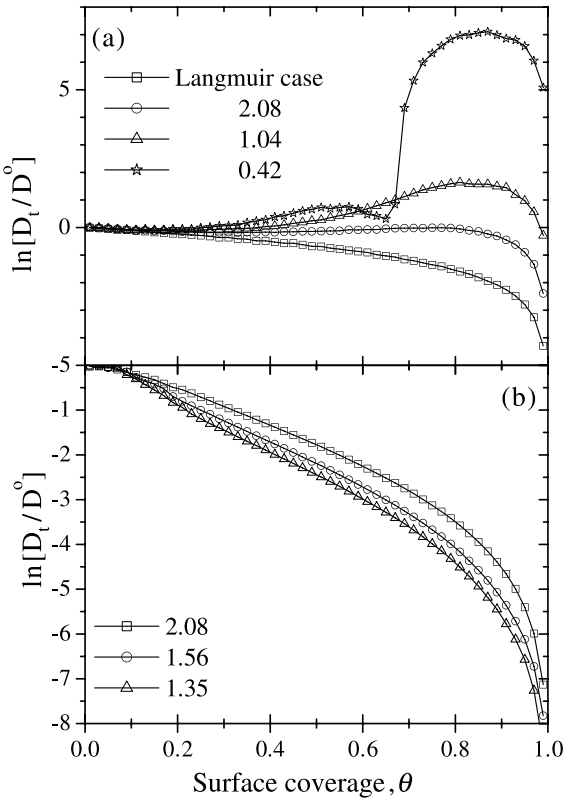

Fig. 8. The coverage dependencies of the tracer diffusion coefficient for different temperatures and three-particle interaction. Notations are the same as in Fig. 4. The data are obtained by the MC method.

D_t, exhibits pronounced minima at the stoichiometric coverages for the pairwise repulsion (see Fig. 7a) and only one minimum is seen at $\theta = \frac{2}{3}$ for the three-particle repulsive interaction (Fig. 8a). This behavior is clearly attributed to the adatom ordering.

Figs. 7b and 8b reflect the behavior of the tracer diffusion coefficient D_t/D^0, for pairwise and three-particle attraction, respectively. As it is clearly seen the surface diffusion process is slow down due to the attractive interaction. In particular, this effect is more pronounced at low temperatures and for high coverages.

It should be noted that we use only MC simulations for investigation the behavior of the tracer diffusion coefficient. In principle, the RSRG approach can be reformulated for investigation the tracer diffusion coefficient. We need to have tagged particles for determining the tracer diffusion coefficient. It can be done using the Blume–Emery–Griffiths model [33]. It is a spin model with $S = 1$. Then, any lattice spin can assume three values 0 and ± 1. In the lattice gas language any site can be empty or occupied by an 'ordinary' particle or by a 'tagged' particle. The diffusion in the mixture of ordinary and tagged particles was investigated in Ref. [34]. Really, the system, equivalent to the Blume–Emery–Griffiths model, is more complex than the Ising model. Therefore, the RSRG transformations are also more complex. On the other hand, the tracer diffusion coefficient is a very suitable quantity for the investigations by MC methods.

The chemical diffusion coefficient, D_c, has been calculated by using Eqs. (6) and (7). Another alternative way of evaluating the chemical diffusion coefficient is the Kubo–Green equation [35]. Thus, D_c, can be also written in the following form

$$D_c = D_J \frac{\theta}{\chi_T}, \tag{11}$$

where D_J is the so-called jump diffusion coefficient or kinetic factor. The jump diffusion coefficient, D_J, is a many particle diffusion coefficient describing the asymptotic behavior of the mean square displacement of the center of mass of the system of adparticles. D_J is defined as [35]

$$D_J = \lim_{t\to\infty} \frac{1}{2dN_a t} \left\langle \left\{ \sum_{i=1}^{N_a} [\vec{r}_i(t) - \vec{r}_i(0)] \right\}^2 \right\rangle. \tag{12}$$

This allows us a different and a direct way for evaluating the chemical diffusion coefficient via MC simulations. Thus, Eq. (12) in conjunction with Eq. (11) were used to calculate D_c by means of MC simulations. Therefore, the purely kinetic method and analytical approach (Eq. (6)) can be compared to demonstrate the reliability of the approximations used for calculating D_c.

It is quite obvious and expected that the coverage dependencies of D_t and D_J are quite similar. In particular, it is known that they are numerically equal if there are no velocity-velocity cross correlation terms. However, they represent different views of the diffusive phenomenon. In fact, the tracer diffusion coefficient describes the motion of

tagged particles on the surface while the jump diffusion coefficient represents the mobility of the center of mass of the system.

The coverage dependencies of the chemical diffusion coefficient, D_c, for some representative values of temperature are shown in Figs. 9 and 10. In the whole range of temperatures considered here, at low coverage $\ln[D_c(\theta)/D^0]$ changes almost linearly with coverage θ, as the mean number of nearest neighbors for any jumping particles is growing on average. It is interesting to note that qualitatively the same behavior is visible at coverages slightly below monolayer coverage. At high coverages the relaxation of density fluctuations proceeds via migration of holes. As a consequence, the diffusion activation energy is proportional to the density of holes, $(1-\theta)$.

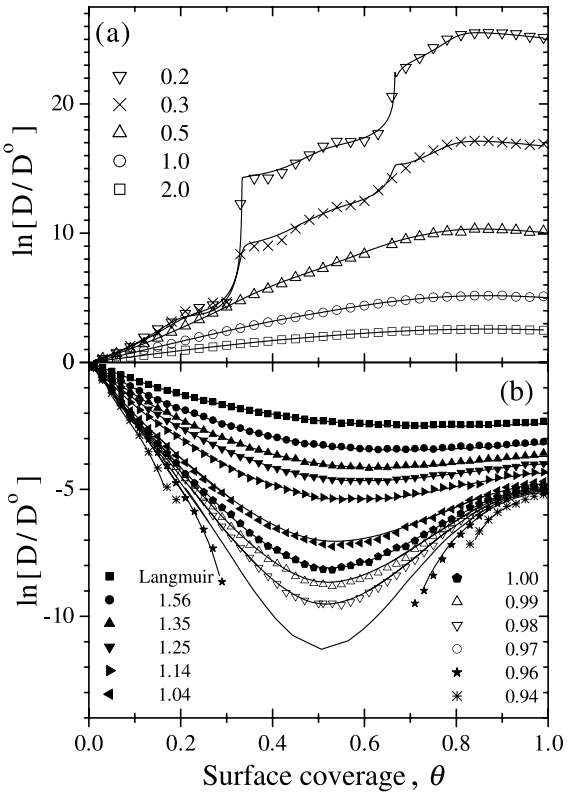

Fig. 9. The coverage dependencies of the chemical diffusion coefficient for different temperatures and pair interaction. Notations are the same as in Fig. 3.

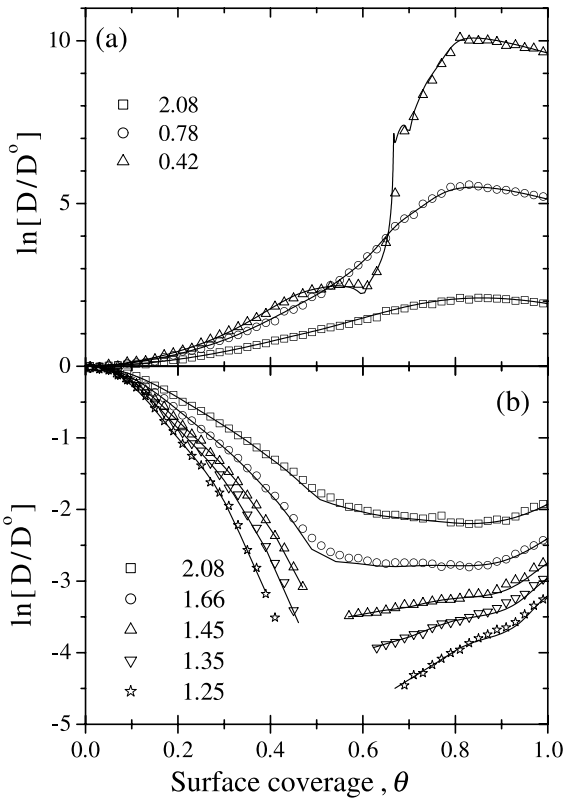

Fig. 10. The coverage dependencies of the chemical diffusion coefficient for different temperatures and three-particle interaction. Notations are the same as in Fig. 4.

The chemical diffusion coefficient grows due to the presence of repulsive interactions, Figs. 9a and 10a. At the critical coverages, the chemical diffusion coefficient exhibits small minima. These minima are related with the peaks of the coverage fluctuations, see Figs. 5a and 6a. At low temperatures the chemical diffusion coefficient changes rather abruptly at the stoichiometric coverages $\theta = \frac{1}{3}$ and $\theta = \frac{2}{3}$ for pairwise repulsion and $\theta = \frac{2}{3}$ for the three-particle repulsive interaction. The jumps of the diffusion activation energy are obviously related to the creation of the ordered phases, which changes considerably the migration of adparticles over surface. For $\theta < \frac{1}{3}$ adparticles migrate over a triangular lattice. The diffusion activation energy is about ε, slightly influenced by the interaction of the jumping particle with its nns. As $\theta \to \frac{1}{3}$ one of the three sublattices becomes

almost completely filled by adparticles. The 1/3 of monolayer occupies one of the three sublattices and the rest of adparticles jump over the honeycomb lattice formed by the other two sublattices. Any adparticle on the honeycomb lattice has three nns. Therefore, the jumps of these adparticle are the most probable and give the main contribution to the surface diffusion. The activation energy is decreased by about 3φ. In fact, the coverage dependencies, $D_c(\theta)$, for $\theta > \frac{1}{3}$ are very similar to the corresponding curves, obtained for the honeycomb lattice [10]. The formation of the AF ordered phase at $\theta = \frac{2}{3}$ is equivalent to the formation of the ordered $c(2 \times 2)$ structure on the honeycomb lattice and causes the same peculiarities on the dependencies of the chemical diffusion coefficient.

For the case of attractive interactions the behavior of the coverage dependencies is determined almost completely by the density fluctuations. As temperature decreases, the fluctuations infinitely grow and cause the slowdown of the diffusion coefficient (see Figs. 9b and 10b). At critical points the diffusion coefficient turns to zero. The critical slowdown is described by Eq. (9).

The fitting between RSRG results and MC data is rather good in the whole range of coverages and temperatures. Even for low temperatures ($T < T_c$) the discrepancies between the different methods are rather small. However, in the vicinities of the critical points there are deviations between RSRG and MC results.

5. Summary

We have investigated 32 RSRG transformations on the triangular lattice with blocks of different size and symmetries. Critical properties for triangular lattice gas system with pair and three-particle attractive and repulsive interactions have been investigated. It has been shown that the precision of the RSRG method depends strongly not only on the number of sites in the block but also on its composition and symmetry. In general the accuracy of the method increases with the number of sites in the block. It is clearly seen from Tables 1 and 2 that the critical parameters of RSRG transformations approach its exact values as the number of spins in block increases. However, this behavior is a non monotone function of L: some blocks give much better results than others with comparable number of sites.

Using the RSRG method, the triangular lattice gas with repulsive and attractive pair and three-particle lateral interactions between adparticles has been explored. The critical parameters coincide rather well with the known values for this system. Adsorption isotherms at different temperatures and coverage dependencies of the thermodynamic factor and the chemical diffusion coefficient at different temperatures have been also calculated. All these quantities have been compared with the corresponding MC simulation results. The coincidence between RSRG and MC data is very good in whole coverage region for different temperatures. Only in the close vicinities of the critical points for the divergent quantities proportional to the second derivatives of the free energy over its variables, such as the thermodynamic factor, the RSRG approach does not give accurate results.

Good coincidence of the RSRG and MC results for the coverage dependencies of the chemical diffusion coefficient obtained in the wide regions of the surface coverage and temperature also means the applicability of the local equilibrium approximation used for the derivation of Eq. (6). There are no visible and systematic discrepancies between the RSRG curves and MC data in the whole range of surface coverage from the smallest possible value up to the maximum monolayer coverage in a wide region of temperatures, excluding the critical points of the system. It is clear that there are some reasons for the divergence between the RSRG and MC data in the vicinities of the critical points. The first is the singular behavior of the thermodynamic quantities. The divergent quantities like isothermal susceptibility and thermodynamic factor are very sensitive to the smallest errors of the critical exponents determined by the RSRG method. The same is also valid for the MC approach. The finite lattice size used for simulations can influence the data accuracy also. Therefore, both methods have decreased accuracy in the critical regions. In fact, it follows from the basic assumptions of the local equilibrium approximation,

that its validity in the critical region is rather questionable.

Summing up all results one can conclude that the RSRG method can be used successfully for determining thermodynamic and kinetic properties of lattice gas and spin systems. In fact, the thermodynamic quantities can be calculated with great accuracy for two dimensional lattice gas systems with strong lateral pair and multiparticle interactions.

Acknowledgements

This work has been supported by the Grant LN00A015 of the MSMT Czech Republic and grant NATO SfP-972523. One of the authors (F.N.) kindly acknowledges financial support by FUNDACION ANTORCHAS Project no. 13887-89 (Argentina) and CONICET (Argentina).

References

[1] G. Zgrablich, in: W. Rudzinsky, W. Steele, G. Zgrablich (Eds.), Equilibria and Dynamics of Gas Adsorption on Heterogeneous Solid Surfaces, Elsevier, Amsterdam, 1996.
[2] W. Rudzinski, D. Everett, Adsorption of Gases on Heterogeneous Surfaces, Academic Press, New York, 1992.
[3] V.P. Zhdanov, Elementary Physicochemical Processes on Solid Surfaces, Plenum, New York, 1991.
[4] G.E. Murch, in: G.E. Murch, A.S. Nowick (Eds.), Diffusion in Crystalline Solids, Academic Press, Orlando, 1984.
[5] A.A. Tarasenko, A.A. Chumak, Fiz. Tverd. Tela. (Leningrad) 24 (1982) 2972, Sov. Phys. Solid State 24 (1982) 1683.
[6] R. Kutner, K. Binder, K.W. Kehr, Phys. Rev. B 23 (1981) 4931.
[7] R. Kutner, K. Binder, K.W. Kehr, Phys. Rev. B 26 (1982) 2967.
[8] A.A. Tarasenko, A.A. Chumak, Fiz. Tverd. Tela. (Leningrad) 22 (1980) 2939, Sov. Phys. Solid State 22 (1980) 1716.
[9] A.A. Tarasenko, A.A. Chumak, Poverkhnost' Fiyika, Khimija, Mekhanika 11 (1989) 98 (in Russian).
[10] A.A. Tarasenko, L. Jastrabik, C. Uebing, Phys. Rev. B 57 (1998) 10166.
[11] A.A. Tarasenko, L. Jastrabik, F. Nieto, C. Ubing, Phys. Rev. B 59 (1999) 8252.
[12] A. Danani, R. Ferrando, E. Scalas, M. Torri, Surf. Sci. 402 (1998) 281.
[13] A. Danani, R. Ferrando, E. Scalas, M. Torri, Int. J. Mod. Phys. B 11 (1997) 2217.
[14] A. Danani, R. Ferrando, E. Scalas, M. Torri, Surf. Sci. 409 (1998) 117.
[15] J.W. Haus, K.W. Kehr, Phys. Rep. 150 (1987) 263.
[16] T. Ala-Nissila, W.K. Han, S.C. Ying, Phys. Rev. Lett. 68 (1992) 1866.
[17] I. Vattulainen, J. Merikoski, T. Ala-Nissila, S.C. Ying, Phys. Rev. Lett. 79 (1997) 257.
[18] A.V. Myshlyavtsev, A.P. Stepanov, C. Uebing, V.P. Zhdanov, Phys. Rev. B 52 (1995) 5977.
[19] F. Nieto, C. Uebing, Ber. Bunsenges. Phys. Chem. 102 (1998) 974;
F. Nieto, A.A. Tarasenko, C. Uebing, Europhys. Lett. 43 (1998) 558–564;
A.A. Tarasenko, F. Nieto, C. Uebing, Phys. Chem. Chem. Phys. (PCCP) 1 (1999) 3437.
[20] A.A. Tarasenko, F. Nieto, L. Jastrabik, C. Uebing, Phys. Rev. B 64 (2001) 075413.
[21] D.A. Reed, G. Ehrlich, Surf. Sci. 102 (1981) 588.
[22] D.A. Reed, G. Ehrlich, Surf. Sci. 105 (1981) 603.
[23] A.A. Chumak, A.A. Tarasenko, Surf. Sci. 91 (1980) 694.
[24] Th. Niemeyer, J.M.J. van Leeuwen, Physica 71 (1974) 17.
[25] M. Nauenberg, B. Nienhuis, Phys. Rev. Lett. 33 (1974) 1598.
[26] B. Nienhuis, M. Nauenberg, Phys. Rev. Lett 35 (1975) 477.
[27] Th. Niemeyer, J.M.J. van Leeuwen, Renormalization theory for Ising-like spin systems, in: C. Domb, M.S. Green (Eds.), Phase Transitions and Critical Phenomena, vol. VI, Academic Press, New York, 1976 (Chapter 7).
[28] G.D. Mahan, F.H. Claro, Phys. Rev. B 16 (1977) 1168.
[29] F. Nieto, A.A. Tarasenko, C. Uebing, Phys. Chem. Chem. Phys. (PCCP) 2 (2000) 3453.
[30] M. Schick, J.S. Walker, M. Wortis, Phys. Rev. B 16 (1977) 2205.
[31] R.J. Baxter, F.U. Wu, Phys. Rev. Lett. 31 (1973) 1294.
[32] C. Domb, Ising model, in: C. Domb, M.S. Green (Eds.), Phase Transitions and Critical Phenomena, vol. V, Academic Press, New York, 1975 (Chapter VI).
[33] M. Blume, V.J. Emery, R.B. Griffiths, Phys. Rev. A 4 (1971) 1071.
[34] A.A. Tarasenko, A.A. Chumak, Ukrainian Phys. J. 37 (1992) 1071.
[35] R. Gomer, Rep. Prog. Phys. 53 (1990) 917.